Desalination and Water Treatment
www.deswater.com

doi: 10.5004/dwt.2022.28004

247 (2022) 132–143
January

Adsorption of Cr(VI) in wastewater by phosphoric acid/nitric acid/oxalic acid modified bagasse

Li Zhang[a], Jing Huang[b], Xuemei Liu[a,*], Simeng Luo[a], Lingxiao Qu[a]

[a]*School of Civil Engineering, East China Jiaotong University, 808 Shuang Gang East Road, Nanchang, Jiangxi 330013, China, Tel. +8613879150240; email: 15797832052@163.com (X. Liu), Tel. +8618339955965; email: 693116111@qq.com (L. Zhang), 1430618379@qq.com (S. Luo), 1050999631@qq.com (L. Qu)*
[b]*Aerospace Kaitian Environmental Protection Technology Co., Ltd., Changsha, Hunan 410100, China, email: 757510366@qq.com*

Received 29 May 2021; Accepted 18 November 2021

ABSTRACT

The heavy metal element chromium in wastewater has great and lasting harm to the environment, it is urgent to control the pollution of Cr(VI) in water. In this work, bagasse was modified by phosphoric acid (PMB), nitric acid (NMB) and oxalic acid (OMB) to adsorb Cr(VI) in wastewater. An orthogonal test was applied to investigate the effects of immersion ratio, immersion temperature, immersion time and acid concentration on the adsorption performance of the adsorbent. The results showed that the adsorption efficiency of the adsorbent was the best under the conditions of immersion ratio of 70:1 [*V*(mL):*m*(g)], immersion temperature of 293 K, immersion time of 4 h and acid concentration of 1 mol L^{-1}. The adsorbents were characterized by scanning electron microscopy, Brunauer–Emmett–Teller method and Fourier-transform infrared spectroscopy. The specific surface area, pore volume and structure of PMB, NMB and OMB were different from that of bagasse. In addition, PMB, NMB and OMB had better Cr(VI) adsorption performance than the original bagasse. The adsorption of Cr(VI) by PMB, NMB and OMB were well demonstrated by Langmuir adsorption isotherm and quasi-secondary kinetic equation. All results show that PMB, NMB and OMB can be used to purify Cr(VI) wastewater effectively.

Keywords: Adsorption; Chromium; Bagasse; Adsorption isotherm; Kinetic equation

1. Introduction

The treatment of heavy metals has become a global interest, and the degree of pollution varies greatly from place to place. Most heavy metals such as cadmium (Cd), lead (Pb), mercury (Hg) and chromium (Cr) are toxic, non-biodegradable, persistent and bio-accumulative. For example, Cr enters the environment mainly through human activities such as Cr salt production, electroplating, production of paints and pigments, etc. Chromium mainly exists in the form of Cr(III) and Cr(VI) in water, and the toxicity of Cr(VI) is 500 times that of Cr(III) [1]. Cr(VI) is more easily absorbed by and accumulates in the human body; it can cause allergies, genetic defects and even cancer. Most industrial wastewater containing chromium is discharged directly without treatment, causing great harm to the ecosystem. Actually, many technologies have been applied to the treatment of Cr(VI) polluted water, such as chemical precipitation, redox, ion exchange, membrane separation, adsorption and electrochemical treatment. Especially, adsorption has been

* Corresponding author.

widely used in the treatment of heavy metal wastewater due to its advantages of simple equipment, wide adaptability and good treatment effect, etc.

Agricultural by-products are a kind of renewable, easily degradable and environmentally-friendly biomass resources [2]. As the main agricultural by-product, straw biomass is widely distributed all over the world, where sugarcane bagasse is a typical representative. Sugarcane belongs to the grass family and is one of the most important sources of sugar production [3]. About 0.3 tons of bagasse can be produced per ton of sugarcane. Bagasse contains a large amount of cellulose, hemicellulose and lignin. Besides, it has a well-developed pore structure and functional groups on the surface, such as carboxyl group, hydroxyl group and amino group, etc, which are conducive to loading heavy metal ions [4]. Bagasse is often used as the basic material for the preparation of adsorbents. After the modification such as chemical processing, physical processing and impregnation, bagasse can be used as a good adsorbent for the removal of heavy metals. The factors affecting the adsorption performance of an adsorbent include specific surface area, pore structure and functional groups [5]. It has been extensively proved that bagasse-based adsorbent materials have a good adsorption performance for heavy metals. Bansal et al. [6] esterified cellulose in bagasse with L-cysteine and applied it to Hg^{2+}-containing simulated wastewater with a maximum adsorption capacity of 116.822 mg g^{-1}, and it satisfied the quasi-secondary kinetics and the Langmuir isotherm equation; Demiral and Güngör [7] found that the maximum removal capacity of Cu-containing wastewater by phosphate-modified bagasse-based activated carbon reached 43.47 mg g^{-1}, in line with the quasi-secondary kinetic model; Sun et al. [8] used bagasse fiber as the raw material, after the esterification reaction of stearic acid, the maximum adsorption capacity for Hg^{2+} reached 178 mg g^{-1}, and a good adsorption effect still remained after six adsorption–desorption cycles. In fact, unmodified bagasse has a poor adsorption effect. Therefore, it needs to be modified to improve the adsorption performance. The acid modification can increase the acidic functional groups on the surface, and can increase the functional groups such as oxygen, nitrogen and sulfur-containing functional groups. Besides, unmodified bagasse can be electrostatically adsorbed, ion-exchanged or chelated with Cr(VI) to achieve the removal effect.

In this study, bagasse will be used as the adsorbent material prepared by phosphoric acid, nitric acid and oxalic acid, and the optimal preparation conditions will be determined by orthogonal test. The Cr(VI) adsorption performance of the adsorbents will be examined, and the adsorption process will be evaluated by adsorption kinetics and the adsorption isotherm model. This research will improve the energy efficiency of bagasse's adsorption of Cr(VI) from wastewater, and provide a theoretical basis and a feasible way to realize the efficient utilization of biomass materials from agricultural and forestry wastes. In addition, the study will provide a theoretical basis for the application of modified biological adsorbents in the treatment of metals in wastewater by exploring the adsorption properties and mechanism of modified bagasse adsorbents on typical heavy metals in wastewater.

2. Materials and methods

2.1. Experimental instruments

The experimental instruments include a scanning electron microscope (Quanta 200 F, FEI, USA), a Fourier Transform Infrared Spectrometer (Vertex 70, Brooke, Germany), an automatic gas adsorption system (ASAP 2020, Mike, The United States), a Ultraviolet-Visible Spectrophotometer (L5S, Shanghai Jingke, China), an electronic analytical balance (AL204, METTLER, Switzerland), a pH meter (pHS-3E, Shanghai Yidian, China), a digital display speed constant temperature shaker (SHZ-82A, Shanghai Zhichu, China), 50 mL colorimetric tube, 1 cm cuvette, volumetric flask, and pipette, etc.

2.2. Setting of experimental factors

2.2.1. Preparation of adsorbents

Original bagasse (OB): Bagasse was acquired from Guangxi. The sugarcane was crushed by a crusher and passed through a 100-mesh sieve, followed by being repeatedly washed with deionized water, and dried at 353 K.

Phosphoric acid-modified bagasse (PMB): at a certain temperature (293, 298, 303 and 308 K), OB was added to a certain concentration (0.1, 0.5, 1.0 and 1.5 mg L^{-1}) of phosphoric acid solution at a certain ratio (50:1, 60:1, 70:1 and 80:1) [*V*(mL):*m*(g)], completely mixed and immersed for a certain period of time (3, 4, 5 and 6 h), then filtered and washed with deionized water to neutral, finally dried at 353 K.

The same procedures were repeated for the preparation of nitric acid-modified bagasse (NMB) and oxalic acid-modified bagasse (OMB).

2.2.2. Influencing factors of adsorption

The main influencing factors of adsorption are pH, the dosage of the adsorbent, adsorption time and initial Cr(VI) concentration. In this experiment, pH was adjusted to 1.0, 2.0, 3.0, 5.0, 7.0, 9.0 and 10.0, respectively; Dosages of the adsorbent were 0.1, 0.2, 0.3, 0.5, 0.7, 0.9 and 1 g, respectively; adsorption time was 30, 60, 90, 120, 150 and 180 min, respectively; Initial Cr(VI) concentration was 10, 30, 50, 70 and 100 mg L^{-1}, respectively. Optimum preparation conditions would be set.

2.3. Characterization of adsorbents

Fourier-transform infrared spectroscopy (FTIR): Using the KBr pellet pressing method, the infrared spectrum of the material was obtained by infrared spectrum scanning. The scanning range was 400~4,000 cm^{-1} and the changes in functional groups were analyzed.

Scanning electron microscopy (SEM): The changes in the surface morphology and pore structure were measured by thermal field emission scanning electron microscopy.

Brunauer–Emmett–Teller (BET): The pore volume and specific surface area of the samples were determined by low-temperature nitrogen adsorption–desorption test. The automatic gas adsorption system was degassed at 333 K for 4 h and then the test was automatically conducted.

2.4. Preparation of simulated wastewater

A 0.2829 g potassium dichromate dried at 393 K for 2 h, dissolved in distilled water, and transferred to a 1,000 mL volumetric flask, then diluted to the mark with distilled water. It was then formulated into simulated wastewater with a concentration of Cr(VI) of 100 mg L^{-1}. The water samples of other concentrations required for the experiment were prepared by diluting the simulated wastewater.

2.5. Adsorption experimental methods

At 298 K, 50 mL Cr(VI) solution of different concentrations was taken, and the pH of the solution was adjusted with 0.1 mol L^{-1} HCl and 0.1 mol L^{-1} NaOH. A certain amount of OB and modified bagasse were added to the solution, and the mixture was shaken in a constant temperature shaker at 120 rpm. After standing for a moment, the solution was filtered and the supernatant was taken to determine the content of Cr(VI) in the solution which was analyzed by an ultraviolet and visible spectrophotometer (Shanghai Jingke Co., Ltd.).

The removal percentage and the amount of Cr(VI) adsorbed by the adsorbents were calculated by Eqs. (1) and (2):

$$R = \frac{C_0 - C_e}{C_0} \times 100\% \tag{1}$$

$$q_e = \frac{\left(C_0 - C_e\right) \times V}{m} \tag{2}$$

where R (%) is the removal rate, C_0 (mg L^{-1}) and C_e (mg L^{-1}) are the initial and equilibrium concentration of Cr(VI), respectively, q_e (mg g^{-1}) is the equilibrium adsorption capacity, V (L) is the volume of the Cr(VI) solution, and m (g) is the weight of the adsorbent used in the experiments.

The experimental data were analyzed by the pseudo-first-order kinetic model, the pseudo-second-order kinetic model and the intraparticle diffusion model. These models can be expressed as:

$$\ln\left(q_e - q_t\right) = \ln q_e - K_1 t \tag{3}$$

$$\frac{t}{q_t} = \frac{1}{K_2 q_e^2} + \frac{1}{q_e} \tag{4}$$

$$q_t = K_{\text{id}} t^{0.5} + C_{\text{id}} \tag{5}$$

where q_t (mg g^{-1}) is the adsorption capacity at time t, K_1 (min^{-1}) is the rate constant of the pseudo-first-order model, K_2 (g mg^{-1} min^{-1}) is the rate constant of the pseudo-second-order model, K_{id} (mg g^{-1} $min^{-0.5}$) is the intraparticle diffusion rate constant, and C_{id} (mg g^{-1}) is the degree of a boundary layer effect.

The experimental data were examined by the Langmuir isotherm and the Freundlich isotherm is given by:

$$q_e = \frac{q_m b C_e}{1 + b C_e} \tag{6}$$

$$q_e = K C_e^{1/n} \tag{7}$$

For the Langmuir isotherm, its basic characteristic can be described by the separation factor R_L as given by:

$$R_L = \frac{1}{1 + b C_0} \tag{8}$$

where q_m (mg g^{-1}) is the saturated adsorption capacity, b (L g^{-1}) is Langmuir constant, which is related to the adsorption intensity, K (μg g^{-1}) and n are Freundlich constants, which are related to the adsorption intensity and adsorption capacity, respectively.

2.6. Data and statistical analysis

The statistical tests were performed using the statistical software package SPSS 16.0. Analysis of variance (ANOVA) was used to test the relative significance of the different treatments through the calculation of their mean differences. Significant differences among means were determined by Duncan's multiple range test at the $p < 0.05$ level. Microsoft Excel 2010 was used for the statistical analysis, and Origin 9.0 and Microsoft Excel 2010 were used to draw the figures.

3. Results and discussion

3.1. Optimum preparation conditions

The factors affecting the preparation of the adsorbent are acid concentration, acidification temperature, impregnation ratio, and carbonization time, by which optimum preparation conditions can be identified. The four preparation parameters were arranged and tested according to the L16 (44) orthogonal table which was slightly adjusted. The acid concentration, immersion temperature, immersion ratio, and immersion time are represented by *A*, *B*, *C*, and *D*, respectively. The factors and levels of the orthogonal test are shown in Table 1. The experimental results are shown in Tables 2–4.

The results showed that the optimum preparation conditions of PMB, NMB and OMB were as follows: at 293 K, OB was added to 1 mol L^{-1} acid solution with a ratio of 70:1 (*V*(mL):*m*(g)), completely mixed and immersed for 4 h. Then, the adsorption experiment was repeated using the adsorbent prepared under this condition. The results showed that the removal rate of Cr(VI) by PMB, NMB and OMB were 91%, 94.6% and 92.2%, respectively, which was larger than the maximum removal rate in the orthogonal test. Therefore,

Table 1
Factors and levels of orthogonal test

Levels	*A* (mol L^{-1})	*B* (k)	*C* (m:v)	*D* (h)
1	0.1	293	50:1	3
2	0.5	298	60:1	4
3	1.0	303	70:1	5
4	1.5	308	80:1	6

Table 2
Orthogonal test results of PMB

Serial number	*A*	*B*	*C*	*D*	Cr(VI) removal rate
1	0.1	293	50:1	3	0.65
2	0.1	298	60:1	4	0.73
3	0.1	303	70:1	5	0.75
4	0.1	308	80:1	6	0.75
5	0.5	298	50:1	5	0.82
6	0.5	293	60:1	6	0.77
7	0.5	308	70:1	3	0.82
8	0.5	303	80:1	4	0.89
9	1.0	303	50:1	6	0.90
10	1.0	308	60:1	5	0.91
11	1.0	293	70:1	4	0.78
12	1.0	298	80:1	3	0.82
13	1.5	308	50:1	4	0.90
14	1.5	303	60:1	3	0.85
15	1.5	298	70:1	6	0.83
16	1.5	293	80:1	5	0.81
K_1	2.88	3.27	3.01	3.14	
K_2	3.30	3.26	3.20	3.30	Factor influence
K_3	3.41	3.18	3.39	3.29	strength $A > C > D > B$
K_4	3.39	3.27	3.38	3.25	
k_1	0.7200	0.8175	0.7525	0.7850	
k_2	0.8250	0.8150	0.800	0.8250	Optimum level:
k_3	0.8525	0.7950	0.8475	0.8225	$A_3B_1C_3D_2$
k_4	0.8475	0.8175	0.8450	0.8125	
R	0.1200	0.0350	0.0825	0.0400	

the condition ($A_3B_1C_3D_2$) was the optimum preparation condition for PMB, NMB and OMB.

3.2. Results of adsorbent characterization

3.2.1. BET analysis

It can be seen from Table 5 that the BET specific surface area of PMB was 5 times that of OB, and the pore volume was 3 times that of OB. Since the hydrogen ions in phosphoric acid contributed to the pore structure through catalysis, phosphate could protect the carbon skeleton from cross-linking collapse, and increase the specific surface area and pore volume [9]. The test result of NMB showed that the specific surface area and pore volume of the adsorbent were smaller than the minimum detection area of the instrument. Thus, it can be suggested that the specific surface area and total pore volume of NMB were less than that of OB, resulting from that the strong acidity of the nitric acid had a strong etching effect on the activated carbon, causing some channels inside the bagasse to be etched by the nitric acid. Some micropores in the bagasse were oxidized and eroded by the nitric acid, and small pores were connected to form large pores, resulting in a decrease in the specific surface area and pore volume of NMB [10]. The BET-specific surface area of OMB was twice that of OB, and the pore volume was 3 times that of OB. This was because oxalic acid had a certain etching effect on the bagasse during the chemical impregnation process, resulting in a change in the skeleton structure, and the internal pores of the bagasse were opened to form micropores, so that the micropore surface area and the micropore volume were increased [10].

3.2.2. SEM analysis

As can be seen from Fig. 1a, OB is a columnar structure, mainly a large pore structure, and the surface is flat. As can be seen from Fig. 1b, the bottom of PMB is honeycomb-shaped, and the whole structure is columnar. The columnar side has a large number of mesopores and micropores, where the mesopores are arranged neatly. NMB is a pleated layer, and a large number of micropores are present on the pleat layer in Fig. 1c. It can be seen from Fig. 1d that OMB is a layered structure doped together, and there are a large number of large pores, and some micropores appear on the bagasse layer, which greatly increased the specific surface area. Combined with BET analysis, it is obvious that these acid modification methods had an effect on the pore walls, causing a great change in the structure, an increase in surface roughness and an increase in wrinkles because of the oxidation property of the acid [12].

3.2.3. FTIR analysis

As can be seen from Fig. 2, for OB, the band at 3,420 cm^{-1} is the O–H stretching vibration of alcohol. The band C≡C at

Table 3
Orthogonal test results of NMB

Serial number	*A*	*B*	*C*	*D*	Cr(VI) removal rate
1	0.1	293	50:1	3	0.65
2	0.1	298	60:1	4	0.69
3	0.1	303	70:1	5	0.72
4	0.1	308	80:1	6	0.72
5	0.5	298	50:1	5	0.80
6	0.5	293	60:1	6	0.80
7	0.5	308	70:1	3	0.83
8	0.5	303	80:1	4	0.92
9	1.0	303	50:1	6	0.92
10	1.0	308	60:1	5	0.93
11	1.0	293	70:1	4	0.80
12	1.0	298	80:1	3	0.83
13	1.5	308	50:1	4	0.94
14	1.5	303	60:1	3	0.86
15	1.5	298	70:1	6	0.85
16	1.5	293	80:1	5	0.82
K_1	2.78	3.31	3.07	3.17	
K_2	3.35	3.28	3.17	3.35	Factor influence strength:
K_3	3.48	3.20	3.42	3.27	$A > C > D > B$
K_4	3.47	3.29	3.42	3.29	
k_1	0.6950	0.8275	0.7675	0.7925	
k_2	0.8375	0.8200	0.7925	0.8375	Optimum level: $A_3B_1C_3D_2$
k_3	0.8700	0.8000	0.8550	0.8175	
k_4	0.8675	0.8225	0.8550	0.8225	
R	0.1750	0.0275	0.0925	0.0450	

1,633 cm^{-1} is the C≡C stretching vibration or C=O stretching vibration in ketone, aldehyde or ester. The band at 1,606 cm^{-1} is assigned to the C=C stretching vibration in carbonyl or aromatic ring, or C=O stretching vibration, and the band at 1,052 cm^{-1} is the –CO stretching vibration. These bands above are common absorption peaks in plant-based materials [13]. The band at 2,926 cm^{-1} indicates the $–CH_2–$ stretching vibration. The band at 1,735 cm^{-1} is –C=O stretching vibration of the carboxylic acid and lactone groups. The band at 1,514 cm^{-1} is the C=C stretching vibration. These are all related to the lignin vibration in bagasse [14]. Besides, the $–CH_2–$ stretching vibration at 1,426 cm^{-1} and the $–CH_3–$ deformation vibration at 1,376 cm^{-1} are the absorption peaks in cellulose and hemicellulose. The bands at 2,373; 2,344 and 1,328 cm^{-1} are assigned to the C–O stretching vibration, the band at 1,249 cm^{-1} is the stretching vibration of the –C–O–C– bond, the band at 1,163 cm^{-1} denotes the C–O stretching or O–H bending vibration in the phenol and carboxyl groups, the band at 834 cm^{-1} indicates the C–H out-of-plane bending vibration, and the band at 605 cm^{-1} is the out-of-plane vibration of $–NH_2$.

After the modification, more oxygenated acidic functional groups were produced due to acid modification. For PMB, NMB and OMB, the intensity of the O–H stretching vibration at 3,420 cm^{-1} of alcohol was strengthened, the intensity of the –C=O stretching vibration of the carboxylic acid and lactone groups at 1,735 cm^{-1} was increased [12,15], and the intensity of bands at 1,514 and 1,163 cm^{-1} were more pronounced. These all indicate an increase of carboxyl, lactone and hydroxyl groups. Therefore, the hydrophilicity of PMB, NMB and OMB was enhanced, and its adsorption effect on Cr(VI) was enhanced.

In addition, due to the different properties of phosphoric acid, nitric acid and oxalic acid, some special functional groups were added after the modification. For example, For PMB, the band at 1,428 cm^{-1} represents P=O, P–O–C or P=OOH, and the band at 1,108 cm^{-1} denotes P–O–P (polyphosphate) [16]; NMB has an asymmetric $–NO_2$ stretching vibration band at 1,513 cm^{-1} [17] and a combined peak of carboxylic acid and nitrate groups appears at 1,381 and 1,332 cm^{-1} [10]. For OMB, the condensation reaction or cleavage of lignin aliphatic side chain due to oxalic acid modification caused the shift and intensity changes of bands at 1,376 and 1,426 cm^{-1}, which was corresponding to the aromatic skeleton vibration, for example, $–CH_2$ and C–C asymmetric bending vibrations [18].

3.3. Factors affecting adsorption

3.3.1. Effect of pH on adsorption

It can be seen from Fig. 3 that the effect of pH on the Cr(VI) removal rate. When the pH value was less than 2, the change rate of Cr(VI) removal rate was small as the pH

Table 4
Orthogonal test results of OMB

Serial number	*A*	*B*	*C*	*D*	Cr(VI) removal rate
1	0.1	293	50:1	3	0.68
2	0.1	298	60:1	4	0.69
3	0.1	303	70:1	5	0.75
4	0.1	308	80:1	6	0.72
5	0.5	298	50:1	5	0.80
6	0.5	293	60:1	6	0.80
7	0.5	308	70:1	3	0.85
8	0.5	303	80:1	4	0.92
9	1.0	303	50:1	6	0.92
10	1.0	308	60:1	5	0.93
11	1.0	293	70:1	4	0.8
12	1.0	298	80:1	3	0.83
13	1.5	308	50:1	4	0.94
14	1.5	303	60:1	3	0.86
15	1.5	298	70:1	6	0.85
16	1.5	293	80:1	5	0.82
K_1	2.84	3.24	3.10	3.22	
K_2	3.37	3.28	3.17	3.35	Factor influence
K_3	3.48	3.25	3.45	3.30	strength $A > C > D > B$
K_4	3.47	3.29	3.44	3.29	
k_1	0.7100	0.8350	0.7750	0.8090	
k_2	0.8426	0.8200	0.7925	0.8375	Optimum level:
k_3	0.8700	0.8125	0.8625	0.8250	$A_3B_1C_3D_2$
k_4	0.8675	0.8225	0.8600	0.8225	
R	0.1600	0.0225	0.0875	0.0325	

Table 5
BET analysis of OB, PMB and OMB

Adsorbent	BET specific surface area ($m^2\ g^{-1}$)	Total pore volume ($cm^3\ g^{-1}$)	Average aperture (nm)
OB	0.8748	0.001564	7.1528
PMB	4.5395	0.004647	4.0946
OMB	1.6463	0.004993	12.13037

increases. When the pH was 1, the Cr(VI) removal rate of OB reached the highest at 57.16%, and the adsorption capacity was 2.041 mg g^{-1}. Then the pH was in the range of 2~10, the Cr(VI) removal rate and adsorption capacity of OB, PMB, NMB and OMB decreased rapidly with the increase of pH. The removal rates of the modified adsorbents were always much larger than OB. When the pH was 2, the adsorption effects of PMB, NMB and OMB reached the highest. The removal rate of PMB, NMB and OMB was 91.0%, 94.6% and 92.3%, respectively; and the adsorption capacity was 3.25, 2.628 and 3.286 mg g^{-1} respectively; Which was 59.24%, 28.76% and 60.99% higher than that of OB, respectively. Harish et al. [19] reported that he maximum percentage removal for synthetic bagasse reached 94.56% values at a pH of 4.0 at 25°C. This removal rate was the same as our study, and the difference in pH is due to the author's use of bagasse that was been made from calcium chloride cross-linked with sodium alginate (Na-Alg). Therefore, we can conclude that the acidic environment is beneficial to the adsorption of Cr(VI) by OB, PMB, NMB and OMB. The adsorption capacity follows the order of OMB > PMB > NMB > OB, and the optimal pH of PMB, NMB and OMB was determined to be 2.

How does pH affect removal rate of Cr(VI)? When the pH is different, chromium exists in different forms in aqueous solution, mainly Cr^{3+}, H_2CrO_4(aq), $Cr_2O_7^{2-}$, $HCrO_4^-$, $KCrO_4^-$ and CrO_4^{2-} [19]. The main forms of chromium ions under acidic conditions are $Cr_2O_7^{2-}$ and $HCrO_4^-$. $HCrO_4^-$ dominates at pH = 1, and $Cr_2O_7^{2-}$ dominates at pH = 2~6. The main form of chromium ion under alkaline conditions is CrO_4^{2-} [20]. Under acidic conditions, H^+ reacted with the surface functional groups of the adsorbent, and chromium exchanged with the cations on the surface of

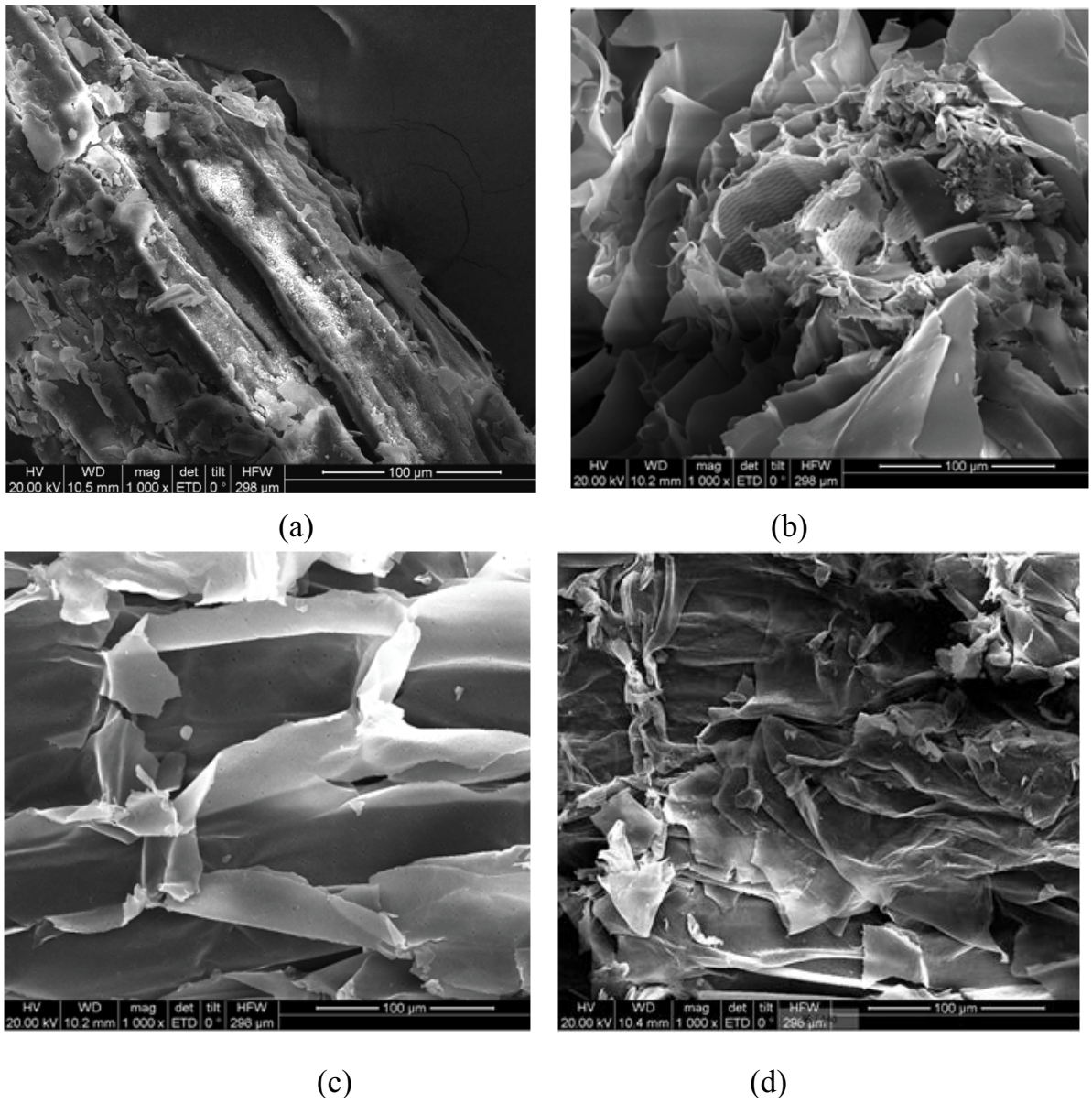

Fig. 1. SEM spectra of (a) OB, (b) PMB, (c) NMB and (d) OMB. SEM means scanning electron microscopy; OB means that modified bagasse; PMB, NMB and OMB means that bagasse was modified by phosphoric acid, nitric acid and oxalic acid to treat Cr(VI)-containing wastewater, respectively.

the adsorbent [21] and electrostatic adsorption was generated, which facilitated the removal of chromium. As the pH increased, the deprotonation reaction occurred, and the OH^- increased, which would compete with the chromium adsorption and hindered the adsorption [22]. Because of the increase in the specific surface area and the change of functional groups, the Cr(VI) adsorption performance of modified bagasse is much better than that of OB.

3.3.2. Effect of adsorbent dosage on adsorption

It can be seen from Fig. 4 that as the adsorbent dosage increases, the Cr(VI) removal rate was continuously enhanced. However, the Cr(VI) removal rate showed a smooth plateau trend when further adsorbents were added. When the dosage of OB was 0.7 g, the Cr(VI) removal rate reached the highest at 56.14%, and the adsorption capacity was 2.005 mg g^{-1}. When the dosage of PMB was 0.7 g, the Cr(VI) removal rate reached the highest at 90.9%, and the adsorption amount was 3.246 mg g^{-1}, which was 61.9% higher than that of OB. When the dosage of NMB was 0.9 g, the Cr(VI) removal rate reached the highest at 94%, and the adsorption amount was 2.611 mg g^{-1}, which is 30.22% higher than that of OB. When the dosage of OMB was 0.7 g, the Cr(VI) removal rate reached the highest at 92.2%, and the adsorption amount was 3.293 mg g^{-1}, which was 64.24% higher than that of OB. Besides, the adsorption capacity decreases with the

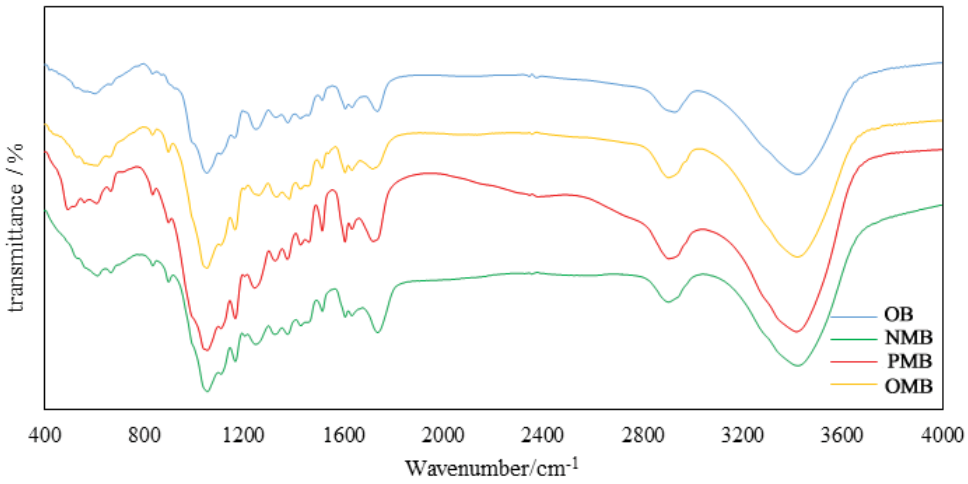

Fig. 2. FTIR spectra of OB, PMB, NMB and OMB. FTIR means Fourier-transform infrared spectroscopy.

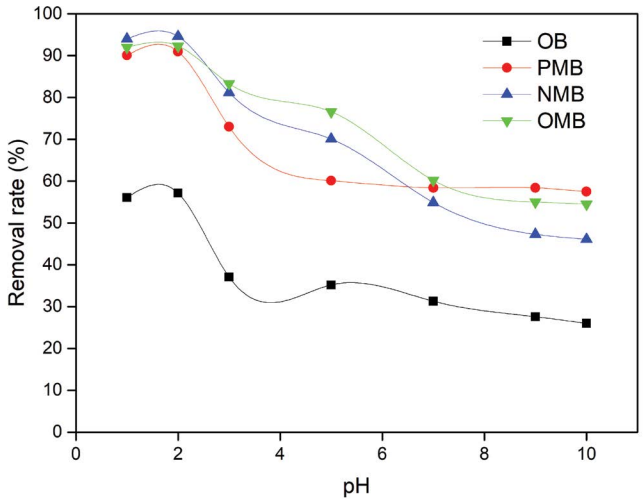

Fig. 3. Effect of pH on Cr(VI) removal rate of OB, PMB, NMB and OMB. That 50 mL simulated wastewater was taken with initial concentration of 50 mg L^{-1}. The rotational speed of wastewater was 120 r min^{-1} and the temperature was 298 K. Experiments were carried out by adding 0.7 g PMB, 0.7 g NMB and 0.9 g OMB inward, respectively.

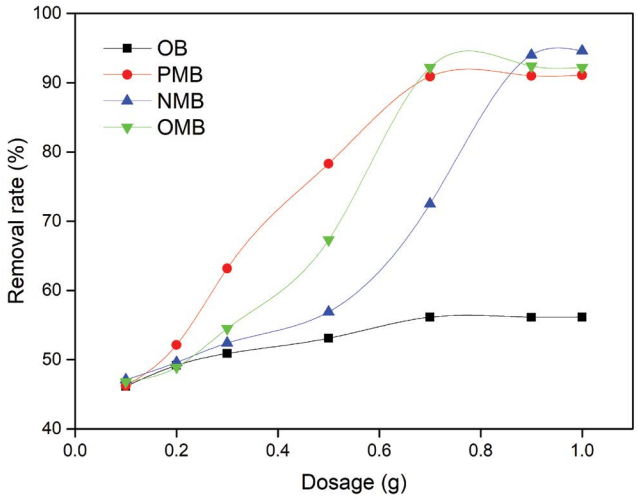

Fig. 4. Effect of adsorbent dosage on Cr(VI) removal rate of OB, PMB, NMB and OMB. That 50 mL simulated wastewater was taken with initial concentration of 50 mg L^{-1} and was added to a conical bottle with pH = 2. The rotational speed of wastewater was 120 r min^{-1} and the temperature was 298 K.

increase of the adsorbent dosage. Therefore, the optimal dosage of OMB and PMB was determined to be 0.7 g, and the optimum dosage of NMB was determined to be 0.9 g for further study. Tan et al. [23] studied the adsorption effect of activated alumina (AA) on hexavalent chromium, the results showed that the removal rate of hexavalent chromium gradually increased with the increase of the amount of activated alumina and then tended to be stable.

The Cr(VI) removal rate was continuously enhanced with the increase of the adsorbent dosage, due to increasing the adsorption active sites by increasing the adsorbent dosage. When the dosage of adsorbent is too high, the activity of the adsorbent surface will be unsaturated, and the interaction between particles (such as agglomeration) will be less, resulting in a decrease in the surface area of the adsorbent and an increase in the particle diffusion path [23,24].

3.3.3. *Effect of adsorption time on adsorption*

It can be seen from Fig. 5 illustrated the effect of adsorption contact time on the adsorption performance of the adsorbents. As the adsorption time increased, the Cr(VI) removal rate continuously increased. However, when the adsorption time reached a certain value, the increase in the adsorption time had no effect on the removal rate. When the adsorption time was 120 min, the removal rate of OB reached the highest at 57.16%, and the adsorption amount was 2.041 mg g^{-1}. When the adsorption time was 120 min, the removal rates of PMB and OMB both reached the highest at

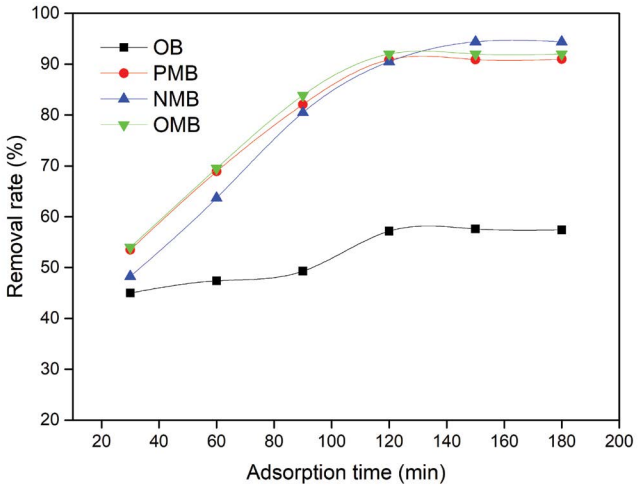

Fig. 5. Effect of adsorption time on Cr(VI) removal rate of OB, PMB, NMB and OMB. That 50 mL simulated wastewater was taken with initial concentration of 50 mg L^{-1} and was added to a conical bottle with pH = 2. The rotational speed of wastewater was 120 r min^{-1} and the temperature was 298 K. Experiments were carried out by adding 0.7 g PMB, 0.7 g NMB and 0.9 g OMB inward, respectively.

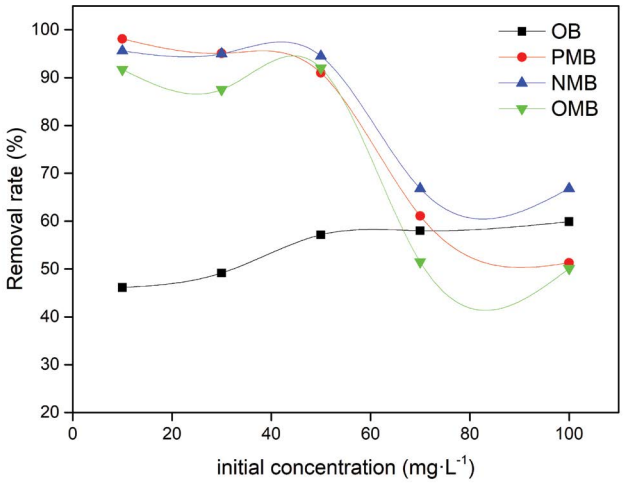

Fig. 6. Effect of initial concentration of wastewater on Cr(VI) removal rate of OB, PMB, NMB and OMB. That 50 mL simulated wastewater was taken and added to a conical bottle with pH = 2. The rotational speed of wastewater was 120 r min^{-1} and the temperature was 298 K. Experiments were carried out by adding 0.7 g PMB, 0.7 g NMB and 0.9 g OMB inward, respectively.

90.9% and 92.0%, respectively. The corresponding adsorption capacity was 3.286 and 3.246 mg g^{-1}, respectively, which was 61.0% and 59.4% higher than that of OB. When the adsorption time was 150 min, the removal rate of NMB reached the highest at 94.4%, and the adsorption amount was 2.622 mg g^{-1}, which was 28.5% higher than that of OB. Therefore, the optimal adsorption time of OMB and PMB was determined to be 120 min, and the optimal adsorption time of NMB was determined to be 150 min. Xu et al. [25] studied the adsorption conditions of modified kaolin by soaking kaolin in ferrous sulfate and by removing hexavalent chromium. The results showed that the optimal conditions for the adsorption of hexavalent chromium were as follows: 0.5 g ferrous sulfate modified kaolin was added, reaction temperature was 30°C, reaction time was 20 min.

3.3.4. Effect of initial Cr(VI) concentration on adsorption

Fig. 6 showed the effect of initial Cr(VI) concentration on the adsorption performance of the adsorbents. It can be seen that when the initial concentration was lower than 50 mg L^{-1}, the Cr(VI) removal rate of PMB, NMB and OMB did not much change with concentration increasing. When the initial concentration was higher than 50 mg L^{-1}, the Cr(VI) removal rate of PMB, NMB and OMB rapidly reduced. Besides, the Cr(VI) removal rate of OB increased slowly with the increase of concentration, but the overall increase was not large. Zhang [26] used sulfuric acid as dehydrating agent to activated carbon and applied to the adsorption of Cr(VI) in wastewater; initial concentration changes from 10 to 120 μg mL^{-1}, when the initial concentration reaches 60 μg mL^{-1}, the maximum adsorption capacity basically remain unchanged.

These phenomena resulted from the fact that when the concentration of Cr(VI) was low, the number of active sites provided by the adsorbent was much larger than the number of active sites in the case of Cr(VI) higher concentration. Therefore, as the concentration of Cr(VI) increased, the removal rate of Cr(VI) by the adsorbent became higher. When the concentration of Cr(VI) exceeded a certain value, the number of available active sites gradually reduced and competitive adsorption occurred. In summary, the optimum initial Cr(VI) concentration was 50 mg L^{-1}.

The analysis of the above four factors shows that under the same conditions, the adsorption properties of PMB, NMB and OMB have been greatly improved compared with those of OB. The results indicate that PMB, NMB and OMB have promising application prospects in the purification of chromium-polluted wastewater.

3.4. Mechanism of adsorption process

3.4.1. Adsorption isotherm

50 mL water samples were used, with initial Cr(VI) concentrations of 10, 30, 50, 70, and 100 mg L^{-1}, respectively. Adsorption was carried out under optimal conditions. The experimental data were analyzed by the Langmuir and Freundlich isotherm models. The results were shown in Table 6. As can be seen from Fig. 7, the adsorption capacity of Cr(VI) by PMB, NMB and OMB would increase as the equilibrium concentration increases. The slopes of the curves in the figure decrease with the increase of the equilibrium concentration, and the final slopes would very close to 0.

It can be seen from Table 6 that the Langmuir isotherm fit best. Langmuir isotherm was based on the assumption that the adsorbent surface is uniform and all adsorption points have the same energy [27]. When the molecules were adsorbed on the surface of the adsorbent to form a

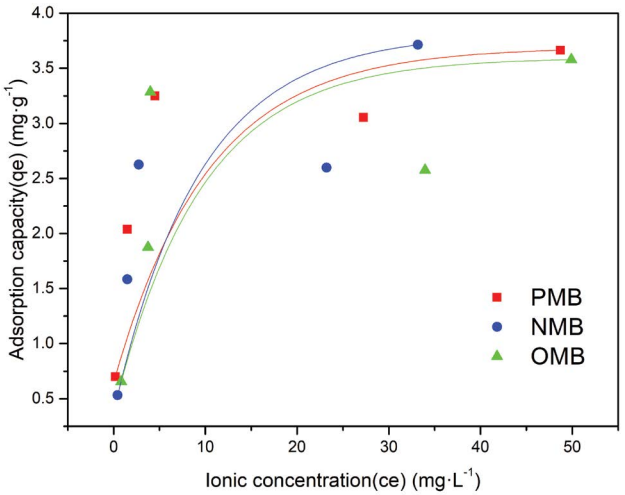

Fig. 7. Isothermal adsorption model of PMB, NMB and OMB. That 50 mL simulated wastewater was taken with initial concentration of 50 mg L^{-1} and was added to a conical bottle with pH = 2. The rotational speed of wastewater was 120 r min^{-1} and the temperature was 298 K. Isothermal adsorption experiments were carried out by adding 0.7 g PMB, 0.7 g NMB and 0.9 g OMB inward, respectively.

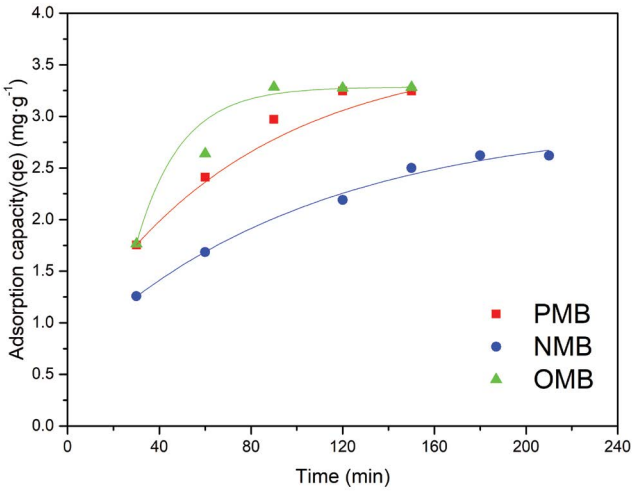

Fig. 8. Adsorption kinetic model of PMB, NMB and OMB. That 50 mL simulated wastewater was taken with initial concentration of 50 mg L^{-1} and was added to a conical bottle with pH = 2. The rotational speed of wastewater was 120 r min^{-1} and the temperature was 298 K. Adsorption kinetics experiments were carried out by adding 0.7 g PMB, 0.7 g NMB and 0.9 g OMB inward respectively.

saturated layer, the largest single-layer adsorption of metal ions occurred [28,29]. Therefore, the Cr(VI) adsorption by PMB, NMB and OMB was mainly single-layer adsorption, and after reaching saturated adsorption, the interaction between the adsorbed chromium ions was negligible. In addition, the separation factor R_L is often used to evaluate the advantages and feasibility of the adsorption process. The adsorption process confirms to be unfavorable ($R_L > 1$), linear ($R_L = 1$), favorable ($0 < R_L < 1$) or irreversible ($R_L = 0$) [30,31]. The calculated results showed that R_L values were between 0 and 1, so the adsorption in this work was favorable. The Freundlich isotherm model describes the non-ideal multilayer adsorption that occurs on non-uniform surfaces. It can be seen from the Table 6 that the calculated $1/n$ value is between 0 and 1, indicating that the Cr(VI) adsorption by PMB, NMB and OMB is the priority [32]. However, the correlation coefficients of this model were 0.8212, 0.7543 and 0.6159, which were a worse fitting result than Langmuir isotherm.

3.4.2. Adsorption kinetics

As can be seen from Fig. 8, the adsorption capacity of PMB, NMB and OMB would increase with time. The adsorption capacity of PMB, NMB and OMB at 30 min reached 54%, 48% and 54%, respectively. The experimental data of PMB, NMB and OMB were analyzed by pseudo-first-order kinetic model, pseudo-second-order kinetic model and intraparticle diffusion model. The results were given in Table 7. It can be seen that the adsorption of Cr(VI) by the three adsorbents did not conform to the pseudo-first-order kinetic model ($R^2 = 0.8651$, $R^2 = 0.84784$, $R^2 = 0.8383$). The analysis showed that the pseudo-first-order kinetic equation was only applicable to the initial stage of the adsorption process, but not to the whole adsorption process. The Pseudo-second-order kinetic model perfectly described the Cr(VI) adsorption of PMB, NMB and OMB ($R^2 = 0.9946$, $R^2 = 0.9952$, $R^2 = 0.9941$). According to the hypothesis of the pseudo-second-order kinetic model, the adsorption process of the three adsorbents was mainly limited by chemical adsorption, which was that the adsorption process was completed by the sharing between electron exchange and adsorbate [14]. In addition, the q_e values calculated by the pseudo-second-order kinetic equation agree well with the experimental values. In order to further determine the diffusion mechanism of the adsorption process, the intraparticle diffusion model was studied. It can be seen from Fig. 8 that the curve of

Table 6
Isotherm parameters of Cr(VI) adsorption of PMB, NMB and OMB

Adsorbent	Langmuir isotherm			Freundlich isotherm		
	q_m (mg g^{-1})	b (L mg^{-1})	R^2	K	$1/n$	R^2
PMB	3.622	0.721	0.9898	1.468	0.273	0.8212
NMB	3.532	0.416	0.9438	1.097	0.359	0.7543
OMB	3.432	0.312	0.9505	1.100	0.317	0.6159

Table 7
Kinetic parameters of Cr(VI) adsorption on PMB, NMB and OMB

Adsorbent	Pseudo-first-order kinetic model			Pseudo-second-order kinetic model		
	q_e (mg g^{-1})	K_1 (min^{-1})	R^2	q_e (mg g^{-1})	K_2 (g mg^{-1} min^{-1})	R^2
PMB	14.929	0.0575	0.8651	4.077	0.007	0.9946
NMB	8.383	0.0368	0.8478	3.230	0.007	0.9952
OMB	52.852	0.0829	0.8383	4.136	0.007	0.9941

intraparticle diffusion model did not pass through the origin, indicating that the intraparticle diffusion was not the only control step and some other factors (such as boundary layer control) might also affect the adsorption. It can be seen from Table 7 that $K_{id,1}$ was the maximum value of the diffusion rate constant, indicating that rapid adsorption played a major role in the entire adsorption process. When the active site on the surface of the adsorbent was completely bound, Cr(VI) was transferred to the interior of the material and bonded to the internal active site. At this time, with the increase of mass transfer resistance, the adsorption rate decreased, that is the adsorption process was slow. Then, the concentration of Cr(VI) and the active sites of adsorbents gradually decreased, and the adsorption rate eventually reached zero which is the adsorption equilibrium [24]. Therefore, the Cr(VI) adsorption of PMB, NMB and OMB was controlled by surface adsorption and intraparticle diffusion. In addition, the values of $C_{id,2}$ and $C_{id,3}$ were higher than $C_{id,1}$, indicating that surface adsorption dominated the entire adsorption process.

4. Conclusion

According to SEM, BET and FTIR analysis, the modification of bagasse was successful. The results showed that under the same conditions, PMB, NMB and OMB were beneficial to the adsorption of Cr(VI), compared with OB. The main conclusions are summarized as follows:

- After modification, the pore volume and specific surface area of PMB and OMB increased, and the pore structure was more developed, which was favorable for adsorption.
- The adsorption process of PMB, NMB and OMB was in accordance with Langmuir adsorption isotherm model, which indicated that the adsorption was monolayer adsorption and preferential adsorption.
- The adsorption kinetic studies showed that the pseudo-second-order kinetic model was more suitable for the adsorption process of PMB, NMB and OMB. Adsorption consisted of three stages, that is, rapid adsorption, slow adsorption and equilibrium adsorption. PMB, NMB and OMB had better Cr(VI) adsorption effect under the combination of surface area, pore volume and functional groups.

Acknowledgments

This study was financially supported by the Science and Technology Support Project of Jiangxi Province (20161BBF60060) and the National Natural Science Foundation of China (41867020).

References

[1] Y.A. Aydın, N.D. Aksoy, Adsorption of chromium on chitosan: optimization, kinetics and thermodynamics, Chem. Eng. J., 151 (2009) 188–194.
[2] M. Omidinasab, N. Rahbar, M. Ahmadi, B. Kakavandi, F. Ghanbari, G.Z. Kyzas, S.S. Martinez, N. Jaafarzadeh, Removal of vanadium and palladium ions by adsorption onto magnetic chitosan nanoparticles, Environ. Sci. Pollut. Res. Int., 25 (2018) 34262–34276.
[3] H. Gao, J. Du, Y. Liao, Removal of chromium(VI) and orange II from aqueous solution using magnetic polyetherimide/sugarcane bagasse, Cellulose, 26 (2019) 3285–3297.
[4] Y. Liu, Q. Yu, J. Xu, Z. Yuan, Evaluation of structural factors affecting high solids enzymatic saccharification of alkali-pretreated sugarcane bagasse, Cellulose, 27 (2020) 1441–1450.
[5] A. Zanchetta, A.C.F. dos Santos, E. Ximenes, C. da Costa Carreira Nunes, M. Boscolo, E. Gomes, M.R. Ladisch, Temperature dependent cellulase adsorption on lignin from sugarcane bagasse, Bioresour. Technol., 252 (2018) 143–149.
[6] M. Bansal, B. Ram, G.S. Chauhan, A. Kaushik, L-Cysteine functionalized bagasse cellulose nanofibers for mercury(II) ions adsorption, Int. J. Biol. Macromol., 112 (2018) 728–736.
[7] H. Demiral, C. Güngör, Adsorption of copper(II) from aqueous solutions on activated carbon prepared from grape bagasse, J. Cleaner Prod., 124 (2016) 103–113.
[8] N. Sun, X. Wen, C. Yan, Adsorption of mercury ions from wastewater aqueous solution by amide functionalized cellulose from sugarcane bagasse, Int. J. Biol. Macromol., 108 (2018) 1199–1206.
[9] G. Chu, J. Zhao, Y. Huang, D. Zhou, Y. Liu, M. Wu, H. Peng, Q. Zhao, B. Pan, C.E.W. Steinberg, phosphoric acid pretreatment enhances the specific surface areas of biochars by generation of micropores, Environ. Pollut., 240 (2018) 1–9.
[10] Y. Gokce, Z. Aktas, Nitric acid modification of activated carbon produced from waste tea and adsorption of methylene blue and phenol, Appl. Surf. Sci., 313 (2014) 352–359.
[11] Z. Fang, H. Liu, Z. Wang, D. Wen, X. Long, Effect of activated carbon modified with oxalic acid on the production of IPA from MX catalyzed by $H_3PW_{12}O_{40}$@carbon and cobalt, J. Ind. Eng. Chem., 68 (2018) 87–98.
[12] Y. Cao, Y. Gu, K. Wang, X. Wang, Z. Gu, T. Ambrico, M.A. Castro, J. Lee, W. Gibbons, J.A. Rice, Adsorption of creatinine on active carbons with nitric acid hydrothermal modification, J. Taiwan Inst. Chem. Eng., 66 (2016) 347–356.
[13] A. Sari, M. Tuzen, Cd(II) adsorption from aqueous solution by raw and modified kaolinite, Appl. Clay Sci., 88–89 (2014) 63–72.
[14] E. Igberase, P. Osifo, Equilibrium, kinetic, thermodynamic and desorption studies of cadmium and lead by polyaniline grafted cross-linked chitosan beads from aqueous solution, J. Ind. Eng. Chem., 26 (2015) 340–347.
[15] A. Zhou, X. Ma, C. Song, Effects of oxidative modification of carbon surface on the adsorption of sulfur compounds in diesel fuel, Appl. Catal., B, 87 (2009) 190–199.

[16] Y. Guo, D.A. Rockstraw, Physicochemical properties of carbons prepared from pecan shell by phosphoric acid activation, Bioresour. Technol., 98 (2007) 1513–1521.
[17] M.M. Keyser, F.F. Prinsloo, Loading of cobalt on carbon nanofibers, Stud. Surf. Sci. Catal., 163 (2007) 45–73.
[18] H. Lee, Y. Seo, J. Lee, Characterization of oxalic acid pretreatment on lignocellulosic biomass using oxalic acid recovered by electrodialysis, Bioresour. Technol., 133 (2013) 87–91.
[19] H.W. Kwak, M.K. Kim, J.Y. Lee, H. Yun, M.H. Kim, Y.H. Park, K.H. Lee, Preparation of bead-type biosorbent from water-soluble *Spirulina platensis* extracts for chromium(VI) removal, Algal Res., 7 (2015) 92–99.
[20] M.K. Gagrai, C. Das, A.K. Golder, Reduction of Cr(VI) into Cr(III) by *Spirulina* dead biomass in aqueous solution: kinetic studies, Chemosphere, 93 (2013) 1366–1371.
[21] H. Chen, G. Dai, J. Zhao, A. Zhong, J. Wu, H. Yan, Removal of copper(II) ions by a biosorbent—*Cinnamomum camphora* leaves powder, J. Hazard. Mater., 177 (2010) 228–236.
[22] C.S. Sundaram, N. Viswanathan, S. Meenakshi, Defluoridation chemistry of synthetic hydroxyapatite at nano scale: equilibrium and kinetic studies, J. Hazard. Mater., 155 (2008) 206–215.
[23] A. Shukla, Y. Zhang, P. Dubey, J.L. Margrave, S.S. Shukla, The role of sawdust in the removal of unwanted materials from water, J. Hazard. Mater., 95 (2002) 137–152.
[24] L. Wu, W. Wan, Z. Shang, X. Gao, N. Kobayashi, G. Luo, Z. Li, Surface modification of phosphoric acid activated carbon by using non-thermal plasma for enhancement of Cu(II) adsorption from aqueous solutions, Sep. Purif. Technol., 197 (2018) 156–169.
[25] L. Xu, M. Wan, S. Li, S. Xu, Z. Zhao, W. Ma, Modified kaolin processing wastewater containing chromium, Shandong Chem. Ind., 48 (2019) 230–232.
[26] Z. Zhang, Adsorption behavior of Cr(Vl) by the activated carbon from corncob residues, J. Anhui Agric. Sci., 47 (2019) 78–82.
[27] Z. Sheng, Y. Shen, H. Dai, S. Pan, B. Ai, L. Zheng, X. Zheng, Z. Xu, Physicochemical characterization of raw and modified banana pseudostem fibers and their adsorption capacities for heavy metal Pb^{2+} and Cd^{2+} in water, Polym. Compos., 39 (2018) 1869–1877.
[28] Z. Wang, J.P. Barford, C.W. Hui, G. McKay, Kinetic and equilibrium studies of hydrophilic and hydrophobic rice husk cellulosic fibers used as oil spill sorbents, Chem. Eng. J., 281 (2015) 961–969.
[29] Z.A. Sutirman, M.M. Sanagi, K.J. Abd Karim, W.A.W. Ibrahim, B.H. Jume, Equilibrium, kinetic and mechanism studies of Cu(II) and Cd(II) ions adsorption by modified chitosan beads, Int. J. Biol. Macromol., 116 (2018) 255–263.
[30] S. Gogoi, R.K. Dutta, Mechanism of fluoride removal by phosphoric acid-enhanced limestone: equilibrium and kinetics of fluoride sorption, Desal. Water Treat., 57 (2016) 6838–6851.
[31] S. He, Y. Li, L. Weng, J. Wang, J. He, Y. Liu, K. Zhang, Q. Wu, Y. Zhang, Z. Zhang, Competitive adsorption of Cd^{2+}, Pb^{2+} and Ni^{2+} onto Fe^{3+}-modified argillaceous limestone: influence of pH, ionic strength and natural organic matters, Sci. Total Environ., 637–638 (2018) 69–78.
[32] Y. Li, J. Zhang, H. Liu, In-situ modification of activated carbon with ethylenediaminetetraacetic acid disodium salt during phosphoric acid activation for enhancement of nickel removal, Powder Technol., 325 (2018) 113–120.